PAPER • OPEN ACCESS

Demonstration of tokamak vertical stability control based on non-inductive Faraday-effect polarimetry measurements

OPEN ACCESS
IOP Publishing | International Atomic Energy Agency
Nuclear Fusion
Nucl. Fusion **66** (2026) 056016 (11pp)
https://doi.org/10.1088/1741-4326/ae5837

Demonstration of tokamak vertical stability control based on non-inductive Faraday-effect polarimetry measurements

T.E. Benedett[1,*], Z.A. Xing[2], J. Chen[1], J. Barr[2], D.L. Brower[1], D. Finkenthal[3], G. Prabhudesai[1], M. Poulos[1] and W.X. Ding[1]

[1] UCLA, Los Angeles, CA 90095 United States of America
[2] General Atomics, San Diego, CA 92186 United States of America
[3] Palomar Scientific Instruments, San Marcos, CA 92069 United States of America

E-mail: benedett@physics.ucla.edu

Received 14 October 2025, revised 22 March 2026
Accepted for publication 27 March 2026
Published 8 April 2026

Abstract

Long-pulse or steady-state fusion reactors are envisioned to control vertical stability based on non-inductive measurements, i.e. that do not rely on temporal change of magnetic field. For the first time, vertical stability control using non-inductive Faraday-effect polarimetry measurements has been demonstrated. The Radial Interferometer-Polarimeter system on DIII-D is capable of microsecond resolution and was used to absolutely determine the vertical position of the plasma magnetic axis Z_0. A vertical stability controller was developed to robustly stabilize diverted plasmas using Faraday-based measurements. The system was able to stabilize against vertical displacement events with growth rates up to 350 s^{-1} in elongated and elliptical plasma shapes, and instabilities with even higher growth rates are likely to be controllable with further improvements to controller tuning. Tests show that the Faraday-based controller remains effective and is capable of recovering from loss of control even when the plasma vertical position is far from the region where the linear model used to calculate Z_0 is most valid. Faraday control has also been activated during plasma ramp-up, demonstrating the robustness of the technique to larger systematic diagnostic uncertainty at low electron density.

Keywords: polarimetry, control, stability, VDE, diagnostics, non-inductive control, Faraday-effect polarimetry

(Some figures may appear in colour only in the online journal)

* Author to whom any correspondence should be addressed.

1. Introduction

Inductive magnetic probes, which measure changes in magnetic field through measuring the current produced in an inductor, have been a mainstay diagnostic in the history of magnetic confinement fusion research for measuring magnetic fields and thus determining plasma shape and position for the purposes of control and analysis. Inductive magnetic probes are used on present-day tokamaks such as DIII-D [1] and are intended for use on ITER [2–6] as the primary technique for measuring magnetic fields, including for their control systems.

However, inductive magnetic probes do face challenges in steady-state or reactor environments. As inductive probes measure changes in magnetic field, the value of the field must be obtained through integration, which is subject to integrator drift [7]. Diagnostics that depend on known resistance or inductance of a circuit can also face the degradation of their sensors due to the thermal and radiation environment of a fusion reactor, resulting in loss of accuracy [8].

Accurate magnetic measurements are important in maintaining plasma control, including against the $n=0$ vertical instability [9], where elongated toroidal plasmas are unstable against vertical displacements. Controlling vertical stability can require millisecond response times to stabilize instabilities with growth rates on the order of 500 s^{-1} in order to avoid disruptions [10]. As such, alternative (non-inductive) techniques with high time resolution for measuring vertical velocity (dZ/dt) are desired for control of plasmas in steady state and/or reactor environments.

Non-inductive measurement techniques include Hall probes, which have been used to stabilize discharges with low elongation (and thus low vertical instability growth rates) for up to two hours on TRIAM-1 M [11, 12]. On TRIAM-1 M, the time resolution of these Hall probes was insufficient to stabilize the plasma during startup, for which inductive measurements were needed. Hall sensors have also been designed as steady-state magnetic probes for ITER, and have been successfully tested against ITER's thermal and radiation environment [7], though with time resolution (50 ms) that is too slow for vertical stability control.

Faraday-effect polarimetry is another non-inductive technique for measuring magnetic fields in tokamak plasmas that has been recognized for the capability to measure the vertical position of the plasma and be applied to vertical stability control [13, 14]. Polarimeters employing vertical chords have been used to find the radial position of the magnetic axis, as on the Madison Symmetric Torus [15, 16]. Faraday-effect polarimetry has been used for plasma control: on TEXTOR, the measurement of the radial position of the magnetic axis obtained via Faraday-effect polarimetry was used for shape control [17] on much slower timescales than vertical stability control requires.

In this paper, following up on measurement work done on EAST [13, 18], Faraday-effect polarimetry is applied to vertical stability control on the DIII-D tokamak, demonstrating the viability of Faraday-effect polarimetry as a method for vertical stability control, and highlighting areas for further study, improvement, and development. The Radial Interferometer-Polarimeter (RIP) diagnostic [19] on DIII-D has time resolution of 0.1 μs [20], which is more than sufficient for vertical stability control. Open questions that will be addressed include whether the plasma core will decouple from the boundary, and whether Faraday-effect polarimetry can stabilize plasmas during ramp-up.

2. Method

2.1. Radial Interferometer-Polarimeter (RIP)

RIP is used to determine magnetic fields in the plasma core of the DIII-D tokamak by measuring the line-integrated Faraday phase and density along three horizontal chords, one at the vacuum vessel center and two others positioned above and below by 13.5 cm, as seen in figure 1.

The Faraday angle φ_F [radians] is defined as

$$\varphi_F = c_F \int n_e B_l \mathrm{d}l \tag{1}$$

where n_e is the electron density [m^{-3}], B_l is the along-chord component of magnetic field [T] (along the probe beams: in this case, $B_l = B_R$, where R is the cylindrical radial coordinate,) and $c_F = 2.62 \times 10^{-13}[T^{-1}]\lambda^2$ is the Verdet constant for the plasma [21], where $\lambda = 461 \times 10^{-6}$ [m] is the wavelength of the electromagnetic radiation of the probe beam.

The Faraday effect is measured [19] through sending right- and left-handed circularly polarized beams colinearly through the plasma, where it strikes a retroreflector and is returned to a detector on the same path. Due to the two polarizations and double-pass, the Faraday effect due to the plasma is one-quarter of the measured phase difference at the detector.

An example of the three-chord Faraday-effect measurements for an example DIII-D shot (shot 200127) is shown in figure 2(*a*): that the $Z = +13.5$ cm chord's measurements are positive while the other two chords' measurements are negative indicates that the sign of B_R differs between them.

Simultaneously, interferometry [19] provides line-integrated density measurements along all three chords:

$$\varphi_I = c_I \int n_e \mathrm{d}l \tag{2}$$

where [21] $c_I = 2.82 \times 10^{-15}$ [m] λ.

RIP data can be used to provide constraints on EFIT [22], as well as magnetic and density fluctuation output with bandwidth of 5 MHz [23], covering MHD [24], turbulence [23] and energetic particle-driven modes (EPMs [25]).

From RIP Faraday and interferometry measurements, a chord-averaged $\bar{B}_R$ can be defined [23] as

$$\bar{B}_R \equiv \frac{\int n_e B_R \mathrm{d}R}{\int n_e \mathrm{d}R} = \frac{c_I \varphi_F}{c_F \varphi_I}. \tag{3}$$

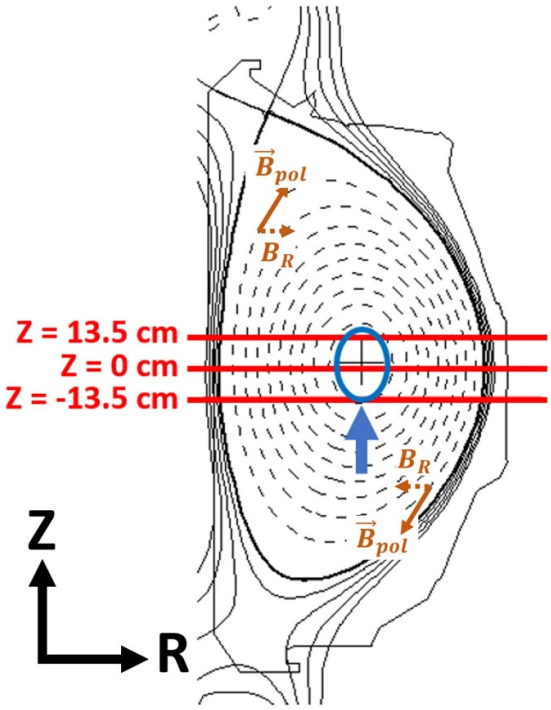

Figure 1. RIP chord locations (red) relative to the DIII-D vessel. Also shown are contours of poloidal flux ψ in an example Grad–Shafanov equilibrium for an experimental shot (shot 202112 at 1500 ms), with a single flux surface highlighted in blue. The point of tangency between the highlighted flux surface and the $z = 13.5$ cm chord is indicated with a blue arrow. Above and below the chords, $\vec{B}_{\rm pol}$ is shown as solid brown arrows, and its radial component (B_R) is shown as dashed brown arrows.

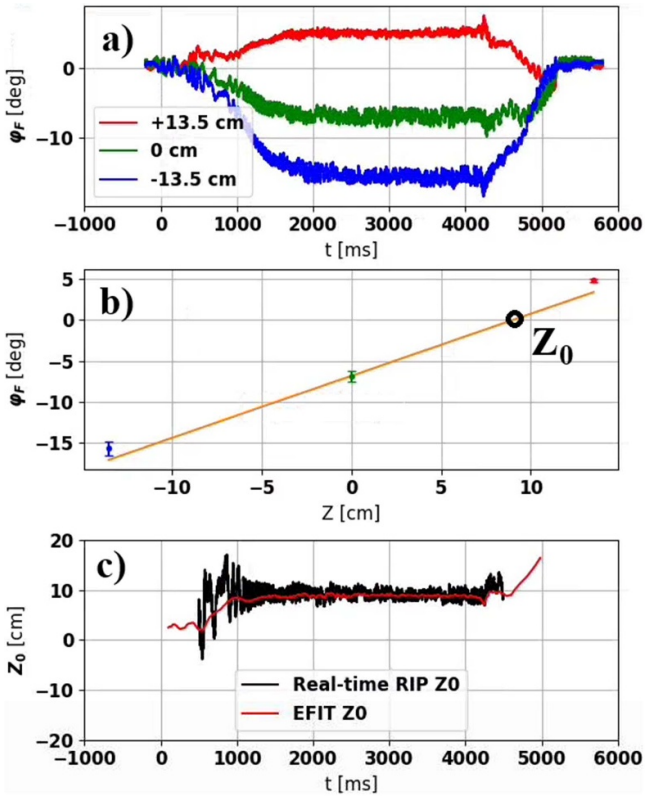

Figure 2. (*a*) Real-time RIP Faraday data versus time for DIII-D shot 200127 (*b*) calculation of Z_0 according to equation (5) for a single point in time $t = 2000$ ms. The three colored points are RIP Faraday data, colored according to chord as in (*a*), and Z_0 is circled in black: $Z_0 = 8.997$ cm. Error bars on the Faraday data are given as ± 1 standard deviation of the value of $\varphi_{\rm F}$ over a $\pm$ 100 ms window. (*c*) Z_0 as calculated in real-time from RIP data (black) and by EFIT (red) for DIII-D shot 200127.

The sightlines pass through or close to the magnetic axis for typical DIII-D plasmas (major radius ≈ 1.67 m, minor radius ≈ 0.67 m, elongation $\kappa \approx 1.9$ [26]). As a result, the equilibrium B_R measurements produced by this diagnostic are core-focused: the component of $\vec{B}$ parallel to the chord is significant only near the magnetic axis, where the chords are tangential to flux surfaces. A point of tangency between a chord and a flux surface is indicated with a blue arrow in figure 1: there, the $z = -13.5$ cm chord is tangent to the highlighted blue flux surface. Along the chords but away from such points of tangency, the equilibrium $\vec{B}$ is nearly perpendicular to the chord direction, as shown by the intersections of the red chords and the dashed-black flux surfaces in figure 1, meaning that the Faraday effect there is negligible.

From RIP Faraday measurements, the vertical position of the magnetic axis and the electron current density on-axis can be determined [18, 27] in real time. This paper will focus on measurement of position for purposes of non-inductive real-time control of plasma vertical velocity.

2.2. Magnetic axis position from polarimetry

Faraday-effect polarimetry can independently produce an absolutely-calibrated measure of the vertical position of the magnetic axis [18]. RIP's three vertically-spaced measurements of the Faraday effect provide information about $\varphi_{\rm F}$ versus vertical position Z at every point in time. Given at least two vertically-spaced measurements of $\varphi_{\rm F}$ taken horizontally near the magnetic axis, a slope $\frac{\Delta\varphi_{\rm F}}{\Delta Z}$ can be obtained, and given a measurement $\varphi_{\rm F_1}$ at vertical position Z_1, the Z-position where $\varphi_{\rm F} = 0$ can be obtained as

$$Z_0 = Z_1 - \frac{\varphi_{\rm F_1}}{\frac{\Delta\varphi_{\rm F}}{\Delta Z}}. \tag{4}$$

Given the three chords of RIP ($Z = 13.5$ cm, $Z = 0$ cm, $Z = -13.5$ cm) $\frac{\Delta\varphi_{\rm F}}{\Delta Z} = \frac{\varphi_{\rm F}(13.5\text{ cm}) - \varphi_{\rm F}(-13.5\text{ cm})}{0.27m}$, and so

$$Z_0 = -\frac{\varphi_{\rm F}(0\text{ cm})}{\varphi_{\rm F}(13.5\text{ cm}) - \varphi_{\rm F}(-13.5\text{ cm})} \times 0.27\text{ m}. \tag{5}$$

As $\varphi_{\rm F} \propto \int n_e B_R {\rm d}R$, and the chords pass through the center of the plasma, the location where $\varphi_{\rm F} = 0$ with $n_e > 0$ means there is no net B_R, i.e. that location Z_0 is the vertical position of the magnetic axis.

This is shown in figure 2(*b*) for a single timeslice ($t = 2000$ ms) of DIII-D shot 200127. The three dots, colored according to chord as in figure 2(*a*), show the polarimetry measurements at that instant. A linear fit (orange line) is applied to find the Z-position of the magnetic axis (circled

in black,) per equation (5). This process, done for 20 000 timeslices per second in real time, produces the black curve in figure 2(*c*), and is compared to the post-shot calculation of the magnetic axis Z-position from EFIT [28] (red curve).

This method for finding Z_0 is valid so long as $\int n_e B_R \mathrm{d}R$ varies approximately linearly with Z; i.e. so long as the magnetic axis is sufficiently close to the measurement locations, which is true for typical DIII-D plasmas and the RIP diagnostic. While the three RIP chords would enable the use of a second-order fit, the deviation from linearity is typically small, as shown in figure 2(*b*), and so a linear fit is preferred for its greater resilience to measurement noise.

The $\pm$13.5 cm chord spacing determines the range over which Z_0 can be accurately determined and was selected based on available port space. This spacing can be optimized for a specific device application.

RIP's Digital Phase Demodulator (DPD [29]) provides real-time phase output for the polarimetry and interferometry measurements at each chord, enabling real-time Z_0 calculation for control applications.

Uncertainty in RIP measurements (visible in the fluctuations of the black curve around the red curve in figure 2) is highest during ramp-up, at the beginning of the shot, due to both low plasma current and density resulting in a small φ_F and a corresponding low signal-to-noise ratio. Internal optical feedback oscillations due to changing density [30] are also strongest during ramp-up; internal optical feedback is discussed in more detail in section 3.4. After ramp-up is complete, during the flattop, (after approximately 1500 ms in figure 2) changes in density are smaller, resulting in less optical feedback, and higher densities and plasma currents result in higher signal-to-noise ratios, reducing RIP uncertainty. Uncertainty in Z_0 during the flattop, as seen in figure 3(*a*), is typically within $\pm$1.5 cm. Investigations of the results of the experiment presented in this paper (section 3.4) indicate that internal optical feedback was not a limiting factor on control performance.

2.3. DIII-D's Plasma Control System (PCS)

DIII-D's PCS [31] is responsible for controlling and stabilizing plasma discharges, and consists of many integrated hardware and software systems. The original analog PCS was digitized in the early 1990s [32] and has been subject to continual improvements and additions. However, many fundamental functions, including vertical stability control, remain emulations of the original analog systems.

Vertical stability control has remained fundamentally the same as it was as of the early 1990s: inductive magnetic measurements are taken and fed into the control system, where $Z_0 I_\mathrm{P}$ (vertical position times plasma current) is computed with a sampling frequency of at least 12.5 kHz, and monitored for fast changes, which, when discovered, are counteracted with poloidal field coil action.

The same actuators as the existing system are used for this experiment, but the measurement technique is changed. As

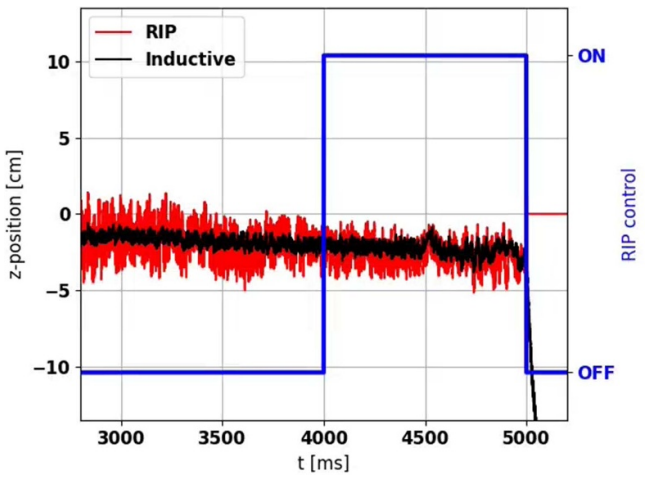

Figure 3. Z_0 as measured by RIP (magnetic axis Z-position, red) and by inductive magnetic probes (current centroid Z-position, black) for DIII-D shot 202790, with RIP control from 4000 to 5000 ms, as shown by the blue trace. Both RIP and magnetic measurements used by the PCS have 20 kHz bandwidth.

such, the method tested here substitutes measurement of the motion of the Z-position of the current centroid as determined with inductive probes with measurement of the Z-position of the magnetic axis as produced by Faraday-effect polarimetry, as in section 2.2.

The signals provided by the DPD are resampled by the PCS at 20 kHz, with latency under 50 μs. Within the PCS, the Z-position of the magnetic axis is calculated per equation (5), and the $Z_0(t)$ measurement is used in a proportional–integral–derivative (PID) controller to direct the poloidal field coil action.

The digital PID controller function in DIII-D's PCS is an emulation of analog PID controllers, and this emulation is used for the RIP-based controller: the PID controller computes a response signal, which is converted into coil commands by a tunable response vector. In contrast, the preexisting inductive-based vertical stability controller neither calculated Z_0 directly nor was it a PID controller.

2.4. Experimental setup

The RIP-based vertical stability control system was tested with a DIII-D experiment that had the primary goal of demonstrating successful vertical stability control using the RIP-based algorithm.

To demonstrate control, the active vertical stability algorithm was to be replaced during a plasma discharge, from the preexisting inductive-based vertical stability controller to the new RIP-based vertical stability controller, with the goal that the plasma should remain stable against vertical displacement events for many instability growth rate times, until the end of the discharge. No other controllers were changed.

The RIP Z_0 controller is a vertical stability controller and is not meant for control of absolute position, although it can be

configured to do so. The absolute position of the magnetic axis is the responsibility of DIII-D's shape controller, a separate subsystem within the PCS. As a consequence, only the derivative term of the PID controller is used for vertical stabilization.

In this experimental test, the derivative gain used in the controller was to be optimized *in situ*. Scans of possible gain values show what value produces optimal behavior, balancing control-induced oscillations with responsiveness.

To test the performance of the controller in maintaining stability in increasingly unstable plasmas, the shape of the plasma was altered (typically to increase elongation) to change the vertical instability growth rate.

3. Results

In this section, final results showing the demonstration of RIP-based vertical stability control will be presented first, in section 3.1, followed by discussion of issues that arose and were resolved before the final results were achieved. Section 3.2 will discuss the discovery and management of control-induced oscillations, while sections 3.3 and 3.4 will discuss two potential causes of control-induced oscillations and how they were both proven not to impede RIP-based vertical stability control. Section 3.5 will discuss a test of control while vertically translating plasmas, and section 3.6 will show a demonstration of RIP-based control during plasma ramp-up.

3.1. Demonstration of non-inductive vertical position control

RIP-based vertical stability control was successfully demonstrated on DIII-D. Figure 3 shows RIP-based control is indistinguishable from inductive magnetic-based control in terms of the behavior of the plasma's Z-position.

Figure 3 shows Z-position of the current centroid as measured by the inductive magnetic probes in black, and the Z-position of the magnetic axis as measured by RIP in red. Vertical stability control is handled by the inductive magnetic controller before 4000 ms, and by the RIP-based controller after 4000 ms, where the changeover is not perceptible in the behavior of the plasma's vertical position.

This successful control was achieved despite controller tuning not being fully optimized for this test. Even so, the foundational features of the controller (RIP measurement of Z_0 and use of RIP measurements for vertical stability control) were demonstrated.

Plasmas with vertical instability growth rates up to 350 s^{-1} were controlled, as demonstrated through a scan of elongation. Figure 4 shows a plot of growth rate (for the n = 0 vertical instability, s^{-1}, in black) versus time for a shot where RIP-based vertical stability control begins at 2000 ms; prior to that, the preexisting inductive-based vertical stability controller was used. The control signal showing when RIP-based control is used is superimposed in blue. The growth rate reaches approximately 350 s^{-1} as of the beginning of RIP control and remains above 300 s^{-1} until the termination of the Ohmic discharge due to exhaustion of V-s after 1900 ms of RIP-based control, more than 500 times the characteristic time of the vertical instability, proving effective RIP-based control. The inductive-based vertical stability controller on DIII-D has been observed [33] to control vertical instabilities with growth rates up to 1000 s^{-1}. Improvement to the record of 350 s^{-1} is expected with further controller tuning optimization.

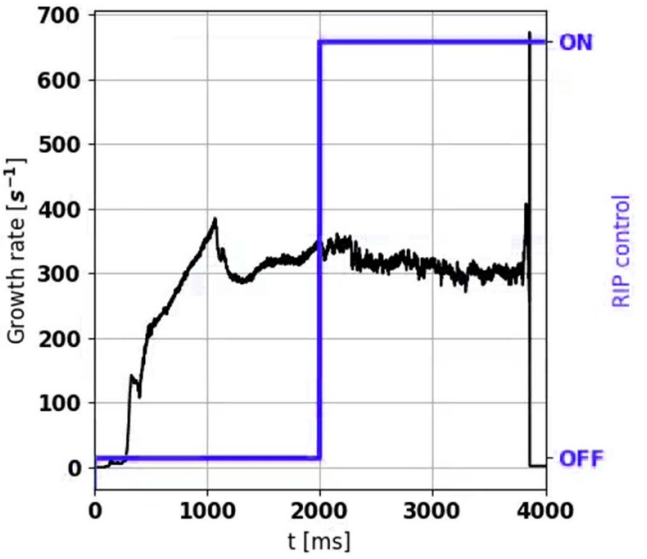

Figure 4. Plot of $n = 0$ instability growth rate for shot 202098 (black), as calculated within the PCS, for a discharge under inductive magnetic control before 2000 ms and RIP control after 2000 ms (control signal shown in blue,) showing control maintained against growth rates of approximately 350 s^{-1}.

3.2. Management of control-induced oscillations

Initially, stronger oscillations were observed under RIP control than under inductive magnetic control. Figure 5 shows a time-trace of Z_0 in (a), and amplitude spectral density plots for the periods under magnetic control (b) and under RIP control (d), as well as phase plots for both periods (respectively (c) and (e)). RIP Z_0 measurements are shown in blue and inductive magnetic Z_0 measurements are shown in orange. Figure 5(a) shows that oscillations in Z_0 are present under magnetic control, but become much stronger under RIP control, The amplitude spectral density plots in figures 5(b) and (d) show that the strongest frequency components of the oscillations are picked up by both RIP and magnetics, both during magnetic control and during RIP control.

It was found that setting $dR_{sep} = 0$ cm (a double-null shape) caused DIII-D's dR_{sep} controller [34] to seek to precisely control Z, and thus give commands to the coils which conflicted with the RIP-based vertical stability controller's commands. Setting $dR_{sep} = -2$ cm avoided this conflict and reduced the amplitude of the oscillations from ± 5 cm to ± 1 cm, but this was not sufficient to reduce the amplitude to levels comparable to that observed under magnetic control. Figure 6 shows the sum of the amplitudes of the 10–300 Hz components of magnetic axis motion integrated over 500 ms both during RIP control (square markers) and during magnetic control (cross markers), indicating that oscillations during RIP control were

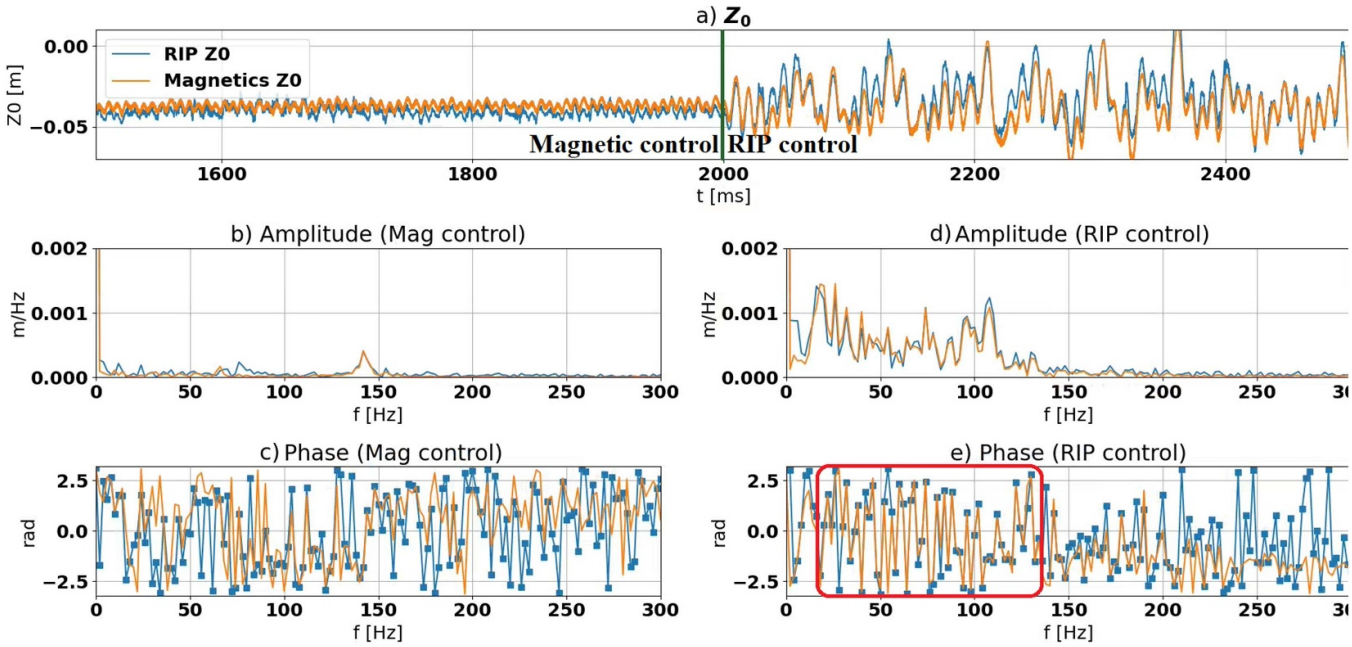

Figure 5. (*a*) Plot of Z_0 in shot 202098 as measured by RIP (blue) and by magnetics (orange), both under magnetic control (before 2000 ms) and under RIP control (after 2000 ms). Amplitude spectral density plots of both the RIP and magnetics Z_0 signals are shown in (*b*) (under magnetic control) and (*c*) (under RIP control), and phase plots for both RIP and magnetics signals are shown in (*d*) (magnetic control) and (*e*) (RIP control). Circled in red in (*e*) is the region of the phase plot corresponding to the strong oscillations observed under RIP control, showing agreement in oscillation phase as measured both by RIP and magnetics.

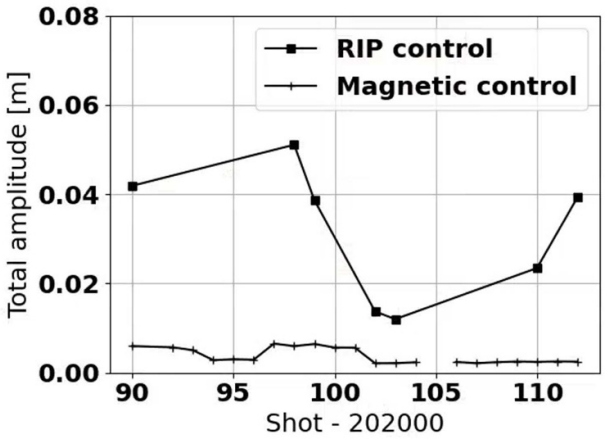

Figure 6. Plot of total oscillation amplitudes from 10 to 300 Hz over 500 ms windows under RIP control (square markers) and under magnetic control (cross markers) versus shot number. Conflict with the shape controller is recognized and avoided beginning at shot 202100, reducing RIP-controlled oscillation levels in shots 202102 and 202103.

initially much stronger than oscillations under magnetic control, but the difference was reduced with improved controller programming. Shots 202110 and 202112 show increased amplitude owing to deliberate linear movement of the plasma during those discharges, picked up as very-low-frequency activity.

Testing of the controller revealed the solution to be the reduction of the τ_D term defining the time window used for the calculation of the derivative in the PID controller within the PCS. As the PCS's PID controller's implementation is an emulation of an analog PID controller, the input signal is also subject to a low-pass filter that produces a phase lag $-\arctan(\tau_D 2\pi f)$ for signal components of frequency f. With $\tau_D = 1$ ms, as was used initially, for $f = 100$ Hz, the phase lag is $-\arctan((0.001\ s)2\pi(100\ \mathrm{s}^{-1})) \approx 0.561$ rad.

Adjusting τ_D to 0.1 ms was found to be sufficient to render the oscillations under RIP control indistinguishable from oscillations under magnetic control (see figure 3). In contrast, increasing τ_D to 3.0 ms resulted in larger-amplitude, lower-frequency oscillations, due to the increased phase lag reducing the responsiveness of the controller.

With the larger oscillations being due to the implementation of the PID controller in DIII-D's PCS, they are not an intrinsic side effect of RIP-based vertical stability control, and can be avoided by using a digital PID controller directly.

Additionally, the growth rate record of 350 s^{-1} (figure 4) was achieved without having resolved the high amplitude of the oscillations under RIP control, suggesting that instabilities with higher growth rates can be controlled with the RIP-based vertical stability controller.

3.3. *Investigation of core-edge decoupling*

Originally, it was thought that the oscillations observed in figure 5 could be due to core-edge decoupling: non-rigid motion of the plasma, which in this case would mean that the RIP measurements of the core would be lagging the coils' action on the plasma boundary, potentially leading to resonance. If present, core-edge decoupling would be a significant

problem for any control method that sought to use core measurements to direct the action of actuators that affect the boundary first, such as RIP-based vertical stability control.

Core-edge decoupling was found to be not the cause of these oscillations through an investigation of the amplitude and frequency spectra of RIP and inductive magnetic measurements of Z_0. Core-edge decoupling would mean that the boundary of the plasma and the magnetic axis were not moving in-phase with each other, and this would be visible as a phase difference at the oscillation frequency between the RIP measurements (which measure magnetic axis Z-position) and the inductive magnetic probes (which measure field at the boundary). Because no such phase difference is seen (see the region of figure 5(*e*) circled in red) core-edge decoupling is not responsible for these oscillations.

3.4. Investigation of internal optical feedback

Another possible cause of the oscillations considered was internal optical feedback in RIP [30].

The double-pass design of RIP, with a zero offset between outgoing and return beams, reduces the probe's footprint but renders it susceptible to internal optical feedback [30], such that changes in density can cause fluctuations in the Faraday-effect measurement about the true phase shift. This is the main systematic error of RIP Faraday measurements.

The dynamic effects of optical feedback are minimized where density changes little with time and the measured Faraday effect is strong, meaning that RIP measurements are most accurate during the flat-top phase of plasma discharges. Designs that spatially separate the outgoing and returning beams, such as ITER's Toroidal Interferometer-Polarimeter [35, 36] can avoid the problem of internal optical feedback, but for this experiment using RIP, the impact of internal optical feedback was usually minimized through testing the controller primarily during the flat-top phase of the discharge. (Tests of RIP-based control before the flat-top are given in section 3.6).

Though the influence of optical feedback was minimized, the $\sim$100 Hz oscillations raised the question of whether its influence had been kept low enough, or whether it produced spurious changes in Faraday measurements sufficient to interfere with vertical stability control. Spurious changes in Faraday measurements could lead to real coils' action and plasma motion, which would be picked up by Faraday measurements, and could resonantly feed back upon itself.

Error in RIP measurements due to internal optical feedback would appear as a phase and/or amplitude difference between the RIP Z_0 measurements and the inductive magnetic Z_0 measurements. If the oscillations were driven by spurious components in the RIP Z_0 measurements, the inductive magnetic measurements would lack that spurious component, resulting in a phase or amplitude difference between RIP Z_0 and inductive magnetic Z_0 at the frequency of the oscillations. Since such phase and amplitude differences are not seen at the frequencies of the main oscillations, again as seen in figure 5, error within RIP measurements is also not a cause of the oscillations. This is the main systematic error of RIP Faraday measurements that has been reduced but not eliminated [30].

3.5. Control in translating plasmas

A test of maintaining vertical stability control over the full extent of the $\pm$13.5 cm range of RIP coverage was performed using the RIP controller. This scan ('triangle waveform scan') involved moving the plasma's magnetic axis up to $Z_0 = 10$ cm and down to $Z_0 = -13$ cm by changing the shape of a diverted plasma, from double-null, to upper-single null, through double-null to lower-single-null, and then back to double-null, as seen in figure 7, in order to ensure that control could be maintained in intentionally translating plasmas, and that control could be maintained while Z_0 was away from 0 (which is where the linear model used to find Z_0 is most valid).

Control was maintained throughout the scan, including the extremes of RIP chord coverage, except for a brief period in the middle of the triangle waveform scan, around $t = 2500$ ms.

The successful control during the majority of the scan demonstrates that RIP-based control is possible in translating plasmas, and is not limited to controlling plasmas with magnetic axis Z-positions in the center of the range of RIP chord coverage, but that control is still possible when the magnetic axis Z-position is at least as far from $Z_0 = 0$ cm as is the upper or lower chord.

During the temporary loss of control at 2500 ms, it can be seen that the plasma was moved up and down rapidly, with the estimates from RIP being exaggerated in magnitude due to the nonlinearity of $\phi_F(Z)$ far from Z_0. EFIT equilibrium calculations failed during the periods of most extreme displacement, but displacement to at least $Z_0 = -27.9$ cm is indicated by the RIP measurements and EFIT reconstructions (see figure 7(*b*)).

Note that RIP data was only used by the vertical stability controller, and neither the shape controller nor EFIT used RIP data: while a Faraday-constrained version of EFIT exists [22], the EFIT results shown in figure 7 were calculated using external magnetic measurements only, and thus the displacements shown here are attested by independent measurements.

This motion brought a region of the plasma into the line of sight of the $Z = +13.5$ cm RIP chord with Faraday effect strong enough to cause fringing in the RIP measurement due to phase wrapping. The phase wrapping can be seen to follow, not precede, the temporary loss of control: see also in figure 7(*c*) at approximately 2430 ms (and the EFIT signals in figure 7(*a*) that large oscillations have begun before any flattening or phase wrapping has appeared in the Faraday signals. The ordering of events shows that anomalies in RIP measurements follow, rather than precede, the oscillations in the plasma, and thus anomalies in RIP measurements are not responsible for the temporary loss of control.

The phase wrapping is also recovered from once the plasma is moved again; this potential for recovery is a benefit of time-independent polarimetric measurements (as contrasted with techniques like interferometry that depend on maintaining an accurate record of phase unwrapping) and from this incident it can be seen that RIP-based vertical stability control is capable of recovering from momentary loss of accurate signal, and also of catching a plasma that has begun to escape from control. As the phase-wrapping pointed out in figure 7(*c*) produces periods where the linear model for Z_0 has the wrong sign (see the

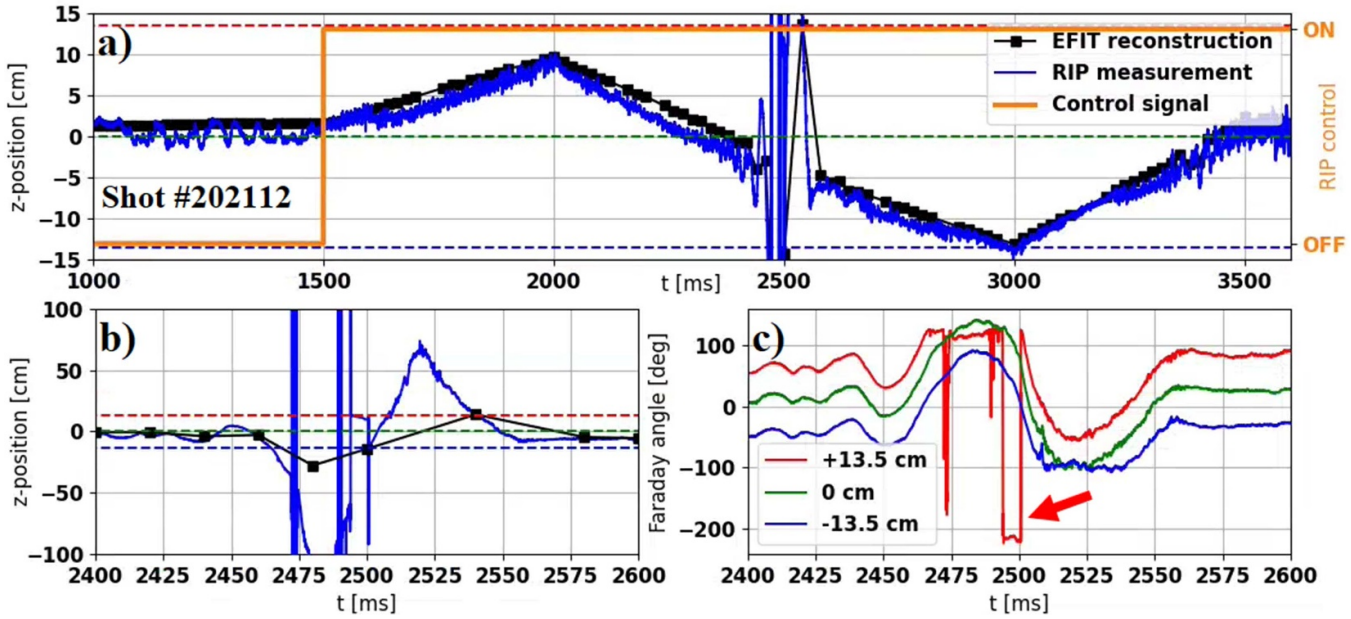

Figure 7. (*a*) *Z*-position of the magnetic axis during a triangle-wave scan controlled by RIP after $t = 1500$ ms (changeover from inductive to RIP control marked with dashed orange trace) as measured in real time by RIP (black) and as calculated by the Grad–Shafranov equilibrium fitting code EFIT (purple). RIP chord positions are marked with horizontal dashed lines. (*b*) Zoom-in in time and zoom-out in space of '(*a*)' during temporary loss of control around 2500 ms. (*c*) Faraday phase measured by the three RIP chords during '(*b*),' showing phase jumps in the $Z = 13.5$ cm chord between 2470 and 2500 ms (red arrow).

vertical spikes in the RIP measurement curve in figure 7(*b*)) in those periods, the RIP-based controller is not the primary system that is controlling the plasma, but is able to restore stability once the anomalous event has passed.

There are two possible causes for the loss of control in this incident: one is that this was the time when the plasma reached maximum elongation, causing the growth rate to reach approximately 350 s^{-1}, which was the maximum observed growth rate in plasmas stably controlled with the RIP-based controller during this first session; control may have been lost with increasing growth rate and recovered as the decreasingly-elongated target shape diminished in growth rate. If this was the cause, losses of control like this can be avoided with improved tuning of the RIP-based controller.

The other possible cause is continued conflict between the control signals provided by the RIP-based vertical stability controller and the dR_{sep} controller used for controlling the shapes of double-null discharges. The oscillation-magnifying conflict was observed prior to this triangle waveform scan and avoided by avoiding the value of $dR_{sep} = 0$ cm, so renewal of that conflict was identified by operators as a possible cause for this behavior that occurred when dR_{sep} crossed from positive to negative. If this was the cause, losses of control like this could be avoided with tighter integration of the RIP-based controller into PCSs. Experimental time was not available to reproduce the plasma shot shown in figure 7 without the dR_{sep} controller active; thus, despite the strong suspicion that controller conflict is the cause, the question is not entirely closed.

3.6. RIP-based control during ramp-up

RIP-based vertical stability control has been successfully used during plasma ramp-up, beginning as early as $t = 280$ ms into the discharge, when the plasma first diverts. This test of RIP control during ramp-up shows that error due to internal RIP feedback (typically strongest during ramp-up) does not inhibit successful control.

Figure 8 shows time-traces of Z_0 (as measured by RIP in blue, and by magnetics in orange) for a discharge under magnetic control until $t = 280$ ms and then under RIP control afterwards, until the termination of the Ohmic discharge. Control is maintained throughout the discharge, though instabilities are continually visible owing to high impurity levels. $t = 280$ ms was the earliest tested changeover time due to being the earliest practical handover time for the tested implementation of the RIP controller in the PCS, and is not an inherent limitation on Faraday-based control.

4. Discussion

Though vertical stability control has been well-handled through the use of inductive magnetic sensors on existing tokamaks, methods based on non-inductive measurements may be of use in steady-state or long-pulse reactors, as they will at least have different strengths and weaknesses compared to inductive probes, and some methods may be found to be more or less susceptible to the extreme conditions of reactor environments than others.

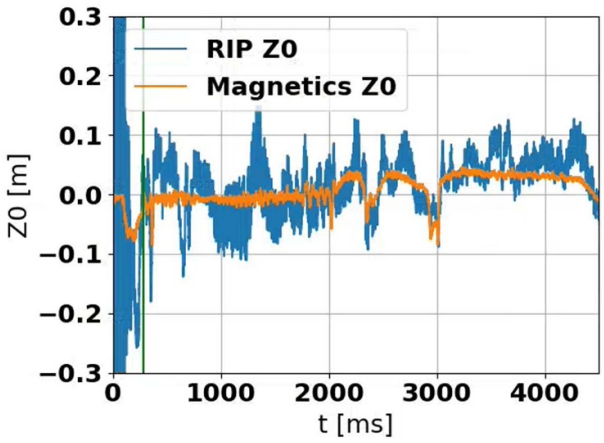

Figure 8. Z_0 for shot 202793 as measured by both RIP (blue) and magnetics (orange), with control handed from magnetics to RIP at 280 ms (green vertical line) and continuing through the end of the discharge.

The primary plasma-facing components in a Faraday-based polarimeter system are mirrors, which are subject to erosion and deposition by contact with the plasma and impurities. Studies of the susceptibility of mirrors to the environment of ITER have been done [37], in which it was found that usable wavelengths may be limited on ITER by mirror survivability concerns, but the exact natures of the threat from the plasma and impurities and of the mitigation methods available will depend on the conditions of the device in question; e.g. a silicon carbide mirror has been found to be appropriate for SPARC [38]. Moving beyond demonstration experiments to steady-state or long-pulse reactors will present more danger and require more solutions.

By contrast, magnetic sensors need not directly face the plasma, but can be shielded, though this has drawbacks, as well, as embedding probes more deeply into the device heightens the cost and effort of replacing them, and also reduces the responsiveness of the sensors, owing to the increased penetration time [3]. Although magnetic coils, as actuators, would also suffer from lower responsiveness on a reactor due to these effects, the use of non-inductive sensors could mitigate this for the vertical control system through providing faster measurements.

It is therefore useful to have non-inductive options available. The method shown in this paper is not as mature as inductive magnetic sensors as applied to control, nor has the RIP system's design been optimized for control, but further testing and refinement is highly likely to improve its capabilities and reliability,so that, if non-inductive measurements are found to be necessary, this method will be available for use.

5. Summary

A non-inductive method based on Faraday-effect measurements for vertical position measurement and control of tokamak discharges, suitable for steady-state applications, has been demonstrated for the first time on DIII-D. The RIP Faraday-effect polarimeter is capable of providing measurements to DIII-D's PCS, which calculates the Z-position of the magnetic axis for use in a PID controller to direct the action of poloidal field coils for stabilizing the plasma against the $n = 0$ vertical instability.

Control has been demonstrated in both stationary and vertically-translating plasmas, and recovery of lost control has been found to be possible, even when the magnetic axis has moved away from the region of greatest accuracy for the linear model used for Z_0 calculation. Plasmas with vertical instability growth rates up to 350 s^{-1} have been stabilized using this method, and this was accomplished with non-optimized tuning and does not represent an upper bound on the method's capabilities.

The RIP-based vertical stability controller has been found to be able to control plasmas during ramp-up, showing resilience against internal optical feedback.

Some difficulties were encountered during the testing of the controller, such as the ∼100 Hz oscillations seen to be consistently stronger under RIP control than under inductive control on the first session of testing, but these were found to be due to specifics of the implementation, including emulation of an analog PID controller, conflict with a shape controller, but not internal optical feedback due to the overlap between the outgoing and return beams, as discussed in section 3, nor were these problems intrinsic to polarimetry-based control. Particularly, the possibility of core-edge decoupling at timescales relevant to vertical stability control was shown to be not present in DIII-D.

Faraday-based vertical stability control can be refined further, as this controller on DIII-D has not been pushed to its limits, and other diagnostic configurations (e.g. separating the outgoing and return beams) offer reduced measurement error and consequently are likely to offer performance gains. Absolute control of Z_0 is expected to be possible, which will likely require integrating the RIP measurements with shape controllers to be most effective. Additionally, Faraday-effect measurements can independently and simultaneously provide more information than just the Z-position of the magnetic axis, such as the current density on the magnetic axis J_0 [27], as well as line-integrated density and real-time measurement of magnetic and density fluctuations, which all have control applications. Thus, Faraday-effect polarimetry presents many reactor-relevant control possibilities.

Acknowledgments

This material is based upon work supported by the U.S. Department of Energy, Office of Science, Office of Fusion Energy Sciences, using the DIII-D National Fusion Facility, a DOE Office of Science user facility, under Awards DE-FC02-04ER54698 and DE-SC0019004.

Disclaimer

ORCID iDs

T.E. Benedett 0000-0001-9888-5545
J. Chen 0000-0002-4853-5341
J. Barr 0000-0001-7768-5931

References

[1] Strait E. 2006 Magnetic diagnostic system of the DIII-D tokamak *Rev. Sci. Instrum.* **77** 023502
[2] Moreau P. *et al* 2009 Development of a magnetic diagnostic suitable for the ITER radiation environment *2009 1st Int. Conf. on Advancements in Nuclear Instrumentation, Measurement Methods and Their Applications* (*Marseille, France*, *7–10 June 2009*) (IEEE) pp 1–8
[3] Humphreys D. *et al* 2009 Experimental vertical stability studies for ITER performance and design guidance *Nucl. Fusion* **49** 115003
[4] Albanese R. *et al* 2009 ITER vertical stabilization system *Fusion Eng. Des.* **84** 394–7
[5] Gribov Y., Kavin A., Lukash V., Khayrutdinov R., Huijsmans G., Loarte A., Snipes J.A. and Zabeo L. 2015 Plasma vertical stabilisation in ITER *Nucl. Fusion* **55** 073021
[6] Ambrosino G., Ariola M., De Tommasi G. and Pironti A. 2011 Robust vertical control of ITER plasmas via static output feedback *2011 IEEE Int. Conf. on Control Applications (CCA)* (*Denver, Colorado, USA*, *28–30 September 2011*) (IEEE) pp 276–81
[7] Kocan M. *et al* 2018 Steady state magnetic sensors for ITER and beyond: development and final design *Rev. Sci. Instrum.* **89** 10J119
[8] Walsh M. *et al* 2011 ITER diagnostic challenges *2011 IEEE/NPSS 24th Symp. on Fusion Engineering* (IEEE) pp 1–8
[9] Lazarus E., Lister J. and Neilson G. 1990 Control of the vertical instability in tokamaks *Nucl. Fusion* **30** 111
[10] Lister J. *et al* 1990 Experimental study of the vertical stability of high decay index plasmas in the DIII-D tokamak *Nucl. Fusion* **30** 2349
[11] Hanada K., Itoh S., Sato K., Nakamura K., Zushi H., Sakamoto M., Jotaki E. and Makino K. 2000 Steady state operation of the superconducting tokamak TRIAM-1M *Steady State Operation of Tokamaks. Proc. Technical Committee Meeting* (*IAEA-TECDOC–1160*) (*Hefei, China*, *13–15 October 1998*) pp 19–27
[12] Itoh S., Sato K. and Nakamura K. 2001 Recent progresses on high performance steady-state plasmas in the superconducting tokamak TRIAM-1M *Technical Report*
[13] Lian H. *et al* 2019 Laser-based Faraday effect polarimetry for real-time feedback control of plasma parameters on EAST *J. Instrum.* **14** C12021
[14] Mazon D. *et al* 2025 Diagnostics: chapter 8 of the special issue: on the path to tokamak burning plasma operation *Nucl. Fusion* **65** 113001
[15] Lin L., Ding W. and Brower D. 2016 Multifield measurement of magnetic fluctuation-induced particle flux in a high-temperature toroidal plasma *Nucl. Fusion* **56** 126020
[16] Lanier N., Anderson J., Forest C., Holly D., Jiang Y. and Brower D. 1999 First results from the far-infrared polarimeter system on the Madison Symmetric Torus reversed field pinch *Rev. Sci. Instrum.* **70** 718–21
[17] Soltwisch H. 1983 Plasma position detection and control in the TEXTOR tokamak by means of a far-infrared interferometer/polarimeter *Nucl. Fusion* **23** 1681
[18] Ding W. *et al* 2018 Non-inductive vertical position measurements by Faraday-effect polarimetry on EAST tokamak *Rev. Sci. Instrum.* **89** 10B103
[19] Chen J., Ding W., Brower D., Finkenthal D., Muscatello C., Taussig D. and Boivin R. 2016 Faraday-effect polarimeter diagnostic for internal magnetic field fluctuation measurements in DIII-D *Rev. Sci. Instrum.* **87** 11E108
[20] Prabhudesai G., Chen J., Brower D. and Finkenthal D. 2024 Upgrade of DIII-D radial interferometer–polarimeter for large bandwidth, low noise and toroidal mode number measurements *Rev. Sci. Instrum.* **95** 093522
[21] Brower D., Ding W., Terry S., Anderson J., Biewer T., Chapman B., Craig D., Forest C., Prager S. and Sarff J. 2003 Laser polarimetric measurement of equilibrium and fluctuating magnetic fields in a reversed field pinch *Rev. Sci. Instrum.* **74** 1534–40
[22] Benedett T., Chen J., Brower D., Yoneda R., Lao L. and McClenaghan J. 2023 Implementing Faraday effect measurement constraints into the Grad–Shafranov equilibrium fitting code EFIT *Rev. Sci. Instrum.* **94** 013507
[23] Chen J. *et al* 2021 Pedestal magnetic turbulence measurements in ELMy H-mode DIII-D plasmas by Faraday-effect polarimetry *Phys. Plasmas* **28** 022506
[24] Pandya M. *et al* 2024 Early internal detection of magnetic tearing and implications for tokamak magnetohydrodynamic stability *Phys. Plasmas* **31** 070706
[25] Lin L. *et al* 2013 Measurement of energetic-particle-driven core magnetic fluctuations and induced fast-ion transport *Phys. Plasmas* **20** 030701
[26] Buttery R. *et al* 2019 DIII-D research to prepare for steady state advanced tokamak power plants *J. Fusion Energy* **38** 72–111
[27] Brower D., Ding W., Terry S., Anderson J., Biewer T., Chapman B., Craig D., Forest C., Prager S. and Sarff J. 2002 Measurement of the current-density profile and plasma dynamics in the reversed-field pinch *Phys. Rev. Lett.* **88** 185005
[28] Lao L., John H.S., Peng Q., Ferron J., Strait E., Taylor T., Meyer W., Zhang C. and You K. 2005 MHD equilibrium reconstruction in the DIII-D tokamak *Fusion Sci. Technol.* **48** 968–77
[29] Colio R., Finkenthal D., Van Zeeland M., Carlstrom T., Gattuso A., Neill R., Boivin R. and Johnson D. 2016 Real-time digital phase demodulator for the ITER toroidal interferometer and polarimeter (TIP) *High Temperature Plasma Diagnostics Conf. (HTPD)* (*Madison, Wisconsin, USA*, *5–9 June 2016*)
[30] Chen J., Ding W., Brower D., Finkenthal D. and Boivin R. 2018 A Faraday-effect polarimeter for fast magnetic dynamics measurement on DIII-D *Rev. Sci. Instrum.* **89** 10B101

[31] Margo M., Penaflor B., Shen H., Ferron J., Piglowski D., Nguyen P., Rauch J., Clement M., Battey A. and Rea C. 2020 Current state of DIII-D plasma control system *Fusion Eng. Des.* **150** 111368
[32] Ferron J., Kellman A., McKee E., Osborne T., Petrach P., Taylor T., Wight J. and Lazarus E. 1991 An advanced plasma control system for the DIII-D tokamak *Technical Report* (General Atomics, San Diego, CA, United States)
[33] Olofsson K. 2022 Fast calculation of the tokamak vertical instability *Plasma Phys. Control. Fusion* **64** 072001
[34] Petrie T. *et al* 2001 The effect of divertor magnetic balance on H-mode performance in DIII-D *J. Nucl. Mater.* **290** 935–9
[35] Kondoh T., Kawano Y., Costley A., Malaquias A., Sugie T. and Walker C. 2003 Toroidal interferometer/polarimeter density measurement system for long pulse operation on ITER *30th EPS Conf. Controlled Fusion and Plasma Physics* (*St. Petersburg, Russia*, *7–11 July 2003*) pp 7–11
[36] Van Zeeland M. *et al* 2018 Tests of a full-scale ITER toroidal interferometer and polarimeter (TIP) prototype on the DIII-D tokamak *Rev. Sci. Instrum.* **89** 10B102
[37] Snider R., Carlstrom T., Hodapp T., Jobes F. and Peebles W. 1997 Application of interferometry and Faraday rotation techniques for density measurements on the next generation of tokamaks *Rev. Sci. Instrum.* **68** 728–31
[38] Song I., Reinke M., Raimond J., Ferrera A., Miner I. and Saltos A. 2024 Design of a multichannel vacuum ultraviolet spectroscopy system for SPARC *Rev. Sci. Instrum.* **95** 083502